

A Time-Dependent Three-Dimensional Dayside Magnetopause Model Based on Quasi-elastodynamic Theory

Yaxin Gu^{1,2}, Yi Wang^{1*}, Fengsi Wei¹, Xueshang Feng¹, Andrey Samsonov², Xiaojian Song³, Boyi Wang¹, Pingbing Zuo¹, Chaowei Jiang¹, Yalan Chen¹, Xiaojun Xu⁴, Zilu Zhou⁴

¹Shenzhen Key Laboratory of Numerical Prediction for Space Storm, College of Aerospace Science and Technology, Harbin Institute of Technology, Shenzhen, 518055, China

²Mullard Space Science Laboratory, University College London, Dorking, RH56NT, United Kingdom

³Shandong High Technology Research, Shandong, 250100, China

⁴State Key Laboratory of Lunar and Planetary Sciences, Macau University of Science and Technology, Macau, 999078, China

*Correspondence to: Yi Wang (wy@hit.edu.cn; wingwy@mail.ustc.edu.cn)

Abstract. The interaction between the solar wind and Earth's magnetosphere is a critical area of research in space weather and space physics. Accurate determination of the magnetopause position is essential for understanding magnetospheric dynamics. While numerous magnetopause models have been developed over past decades, most are time-independent, limiting their ability to elucidate the dynamic movement of the magnetopause under varying solar wind conditions. This study introduces the first time-dependent three-dimensional magnetopause model based on quasi-elastodynamic theory, named the POS (Position-Oscillation-Surface wave) model. Unlike existing time-independent models, the POS model physically reflects the dynamic responses of magnetopause position and shape to time-varying solar wind conditions. The predictive accuracy of the POS model was evaluated by using 38,887 observed magnetopause crossing events. The model achieved a root-mean-square error of 0.774 Earth radii (R_E), representing a 17.9% improvement over five widely used magnetopause models. Notably, the POS model demonstrated superior accuracy under highly disturbed solar wind conditions (22.1% better) and in higher latitude regions (27.0% better) and flank regions (33.3% better) of the magnetopause. The POS model's remarkable accuracy, concise formulation, and fast computational speed enhance our ability to predict magnetopause position and shape in real-time. This advancement is significant for understanding the physical mechanisms of space weather phenomena and improving the accuracy of space weather forecasts. Furthermore, this model may provide new insights and methodologies for constructing magnetopause models for other planets.

1 Introduction

The magnetopause, the boundary between the interplanetary magnetic field (IMF) and Earth's magnetic field, plays a crucial role in space weather forecasting and understanding solar wind-magnetosphere coupling mechanisms (Willis, 1971; P. Song, 1996; Russell, 2003). It acts as a protective shield against hazardous energetic particles while simultaneously serving as the primary interaction region for solar wind-magnetosphere coupling. The magnetopause exhibits considerable dynamic behaviour due to continuous solar wind variations and various instabilities, even under steady solar wind conditions (Anderson et al., 1968; Song et al., 1988; Eastwood et al., 2015). These dynamics can lead to radiation belt particle loss, field-aligned current intensification, ultra-low frequency wave generation, and solar wind energy conversion into the radiation belts, polar regions, and ionosphere (Haerendel, 1990; Mann et al., 2012; Plaschke, 2016; Mottez, 2016; Archer et al., 2019). Consequently, comprehending the interactions between solar wind and magnetopause is vital for advancing magnetosphere dynamics and improving space weather prediction capabilities (Feng, 2020; Zong et al., 2020).

Numerous magnetopause models have been established over the past few decades, generally categorized as physical (or principal) models (Ferraro, 1952; Beard, 1960; Spreiter et al., 1966) and empirical models (Fairfield, 1971; Tsyganenko, 1989; Shue et al., 1998; Lin et al., 2010). Physical models are primarily based on the classic Chapman-Ferraro theory proposed in the 1930s (Chapman and Ferraro, 1930), which states that the magnetopause's equilibrium position is determined by the pressure balance between solar wind dynamic pressure (P_{dyn}) and magnetospheric magnetic pressure (P_b). Since the 1960s, the launch of numerous satellites has provided us with a large number of samples of magnetopause crossing events (MCEs), thereby creating the possibility for the establishment of empirical models (Fairfield, 1971; Sibeck, 1991; Petrinec and Russell, 1996; Shue et al., 1998; Lin et al., 2010). Many empirical models rely on two key parameters, P_{dyn} and IMF B_z , and some of them include the Earth's dipole tilt angle (Φ) to calibrate the higher latitude zone. Besides, some empirical models, proposed from the 1980s, combine physical processes of solar wind-magnetosphere interactions with satellite observation fitting and involved the impact of magnetospheric currents system (Tsyganenko, 1989; Tsyganenko, 1996). Regardless of the assumptions on which these models are based, all these models have contributed to our understanding of magnetopause movement and its response to solar wind conditions. In particular, many of them have been widely used in the prediction of the magnetopause due to their simple form and high prediction accuracy.

However, it should be aware that these models primarily describe the average steady-state characteristics of the magnetosphere. To accurately describe the dynamic coupling process of solar wind-magnetosphere interaction, it is essential to incorporate time partial derivatives into the dynamic equations (Smit, 1968; Petrínek, 2001; Borovsky and Alejandro Valdivia, 2018). This approach, however, complicates the solution of model equations, often necessitating numerical simulations such as magnetohydrodynamics (MHD) (Powell et al., 1999; Raeder et al., 2001; Lyon et al., 2004; Tóth et al., 2005; Merkin and Lyon, 2010), particle-in-cell (PIC) (Moritaka et al., 2012; Ashida et al., 2014; Walker et al., 2019), and hybrid simulations (Gargaté et al., 2008; Omelchenko et al., 2021; Ala-Lahti et al., 2022). Numerical simulations are widely used in exploring solar wind-magnetosphere coupling and can accurately reveal the position of the magnetopause changing with the time-varying solar wind. Collado-Vega et al. (2023) compared the magnetopause predictions obtained by different MHD models, showing the discrepancies for the standoff position. Their analysis also specifically addressed the impact of extreme solar wind conditions, which are known to cause space weather hazards, on the magnetopause. However, the introduction of time partial derivatives makes equations very difficult to solve. In addition, many prominent numerical simulation models may not include properly all magnetospheric current systems (e.g. the ring current or the magnetospheric-ionospheric currents), therefore, this may result in systematic errors of the magnetopause prediction (Samsonov et al., 2016). Moreover, numerical models are solved on supercomputers, consuming a significant amount of computing resources and time, rendering them impractical for real-time space weather forecasting (Raeder et al., 2001; Lyon et al., 2004; Tóth et al., 2005; Feng, 2020). This limitation highlights the need for more **efficient yet accurate** magnetopause models that can capture the dynamic nature of the magnetopause while remaining computationally feasible for real-time applications. Such models would significantly enhance our ability to predict and understand space weather phenomena, bridging the gap between theoretical understanding and practical forecasting capabilities.

Apart from numerical simulations, very few time-dependent magnetopause models have been historically developed (Smit, 1968; Børve et al., 2011; Freeman et al., 1995; Sato et al., 2022). **错误!未找到引用源。** illustrates the fundamental difference between time-independent and time-dependent models. In time-independent models, the magnetopause position is directly correlated with instantaneous solar wind conditions. For example, a step-like increase in solar wind dynamic pressure (such as a shock) corresponds to an immediate step-like compression of the magnetopause (**Figure 1a**). However, this simplification fails to capture the real dynamics of the magnetopause. In reality, the magnetopause undergoes a more

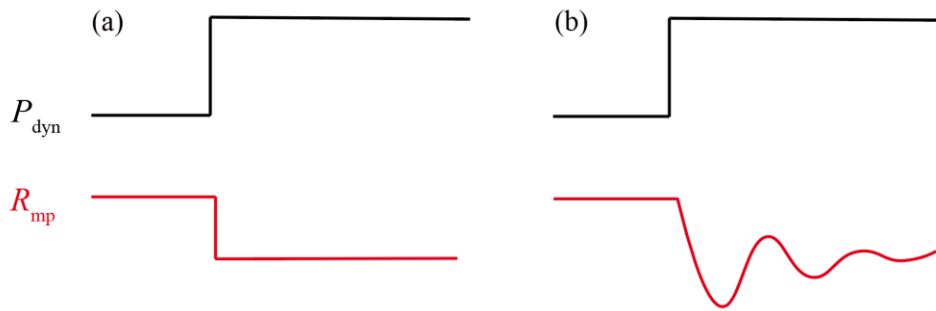


Figure 1: The schematic diagram of time-independent (a) and time-dependent (b) magnetopause models.

Smit (1968) conceptualized the magnetopause as a rigid surface and attempted to explain its motion from the perspective of periodic vibration; Freeman et al. (1995) investigated the influence of inertial and damping effect on the magnetosphere, employing magnetohydrodynamics to analyse the magnetopause motion; Børve et al. (2011) set up a non-adjustable model to analyse the oscillation period of the magnetopause. By investigating the movement of the subsolar point in response to time-varying solar wind, these models are primarily constructed to elucidate specific physical phenomena linked to solar wind-magnetosphere interaction, yet they lack the capability to provide a real-time depiction of the three-dimensional magnetopause position and shape.

Hence, the challenge of constructing time-dependent models lies in balancing the need for accurate dynamic representation with computational feasibility. Although time-dependent models offer a more realistic depiction of magnetopause behaviour, their complexity has limited their development and application, particularly in three-dimensional space. This highlights the necessity for new strategies that can capture time-dependent dynamics while ensuring practical utility for computation, especially for real-time space weather forecasting and related magnetospheric research. Previously, our work revealed the quasi-elastodynamic processes involved in the interaction between solar wind and magnetosphere (Gu et al., 2023). It suggests that the dynamic behaviour of each point on the magnetopause can be viewed as an equilibrium position

(P), radial global oscillations around equilibrium position (O), and surface wave-like structure around the flank regions (S). This work offers a practical framework for developing a time-dependent three-dimensional magnetopause model. However, our previous work primarily focused on elucidating the quasi-elastic process, with less emphasis on the outcomes of model predictions (Gu et al., 2023). Key factors influencing magnetopause dynamics, such as the IMF B_z and Earth's dipole tilt angle (Φ), were not incorporated. Additionally, the adjustable parameters in the equations were simply chosen and lack of thorough calibrations. Moreover, both our prior work and most published magnetopause models (Petrinec and Russell, 1996; Shue et al., 1998; Gu et al., 2023) relied on a relatively limited dataset of low-latitude satellite observations, leading to constraints in accurately representing the higher latitude and flank regions of the magnetopause. To address these limitations and overcome the inherent shortcomings of time-independent models, particularly their inability to reflect the dynamic responses of the magnetopause position and shape to time-varying solar wind conditions, we propose a time-dependent three-dimensional magnetopause model. This model, which has been tested with the largest dataset of MCEs to date (38,887 events), demonstrates remarkable prediction accuracy compared to five widely used magnetopause models. Besides, it offers unparalleled real-time computation speed and a concise form relative to numerical simulations. We have named this model the Position-Oscillation-Surface wave (POS) model.

2 Dataset and other magnetopause models for comparison

The THEMIS (Time History of Events and Macroscale Interactions during Substorms) mission (Angelopoulos, 2008), which consists of five spacecrafts launched into similar elliptical, near-equatorial orbits in 2007, has significantly enhanced our ability to observe the magnetosphere. The mission provides high-resolution (~ 3 s) magnetic field measurements through the THEMIS/Flux Gate Magnetometer (FGM) (Auster et al., 2008) and plasma data from the THEMIS/electrostatic analyser (ESA) (Mcfadden et al., 2008). The Cluster II mission (Escoubet et al., 2001), involving four identical spacecraft launched in 2000, also offers high-resolution (~ 4 s) magnetic field measurements using the CLUSTER/Flux Gate Magnetometer (FGM) (Balogh et al., 1997) and particle data and moments from the Cluster Ion Spectrometry Hot Ion Analyser (CIS-HIA) (Rème et al., 1997).

The WIND spacecraft, launched into orbit around Earth in 1994 and relocated to Lagrange L1 point after 2004, provides continuous, high-quality in-situ solar wind observations. This study utilizes high-resolution (~ 3 s) plasma data from the WIND/3D Plasma Analyzer (3DP) (Lin et al., 1995) and magnetic field data from the Magnetic Field Investigation (MFI)

(Lepping et al., 1995) for upstream solar wind observations. For this study, we have compiled a dataset consisting of 51,590 THEMIS MCEs and 38,321 Cluster MCEs. After excluding redundant crossings (i.e., those occurring simultaneously on the same satellite), invalid data (i.e., crossing without valid upstream solar wind observations), and nightside MCEs (where $X_{\text{GSM}} < 0 R_E$), a total of 38,018 THEMIS MCEs and 869 CLUSTER MCEs (see 错误!未找到引用源。) are selected for this study. The time shift (δt) between WIND to the satellite MCE is determined by comparing the time of each crossing (t_1) with the probable arrival time of corresponding solar wind observation from WIND ($t_0 + \delta t$), satisfying $(t_0 + \delta t) - t_1 < 300$ s. The 300s threshold is set as the potential error window for the time shift from L1 to the magnetopause. δt is calculated as $(L1-r)/\langle v_x \rangle$, L1 ($L1=235 R_E$) is the distance from the Earth to the L1 point, r denotes the radial position of the magnetopause, and $\langle v_x \rangle$ is the 1-hour sliding average of the solar wind velocity in the x-component(Chao et al., 2002). A summary of these events is provided in 错误!书签自引用无效。 . The distribution of matched solar wind conditions for MCEs is shown in Figure 3. All the data is available in the CDAWeb database (<http://cdaweb.gsfc.nasa.gov/>), and the time resolution of the magnetic field and plasma data used in the study is interpolated into 3 seconds, set in GSM coordinates.

Table 1 Summary of collected 89,911 satellite MCEs and dataset used in this paper

Dataset	Satellite	Time interval	Number of datasets
Song et al. (2021)	THEMIS	2007-2022	17,647
Staples et al. (2020a)	THEMIS	2007-2016	33,943
Grimmich (2024)	CLUSTER	2001-2020	38,321
In this paper	THEMIS/CLUSTER	2004-2022	38,887

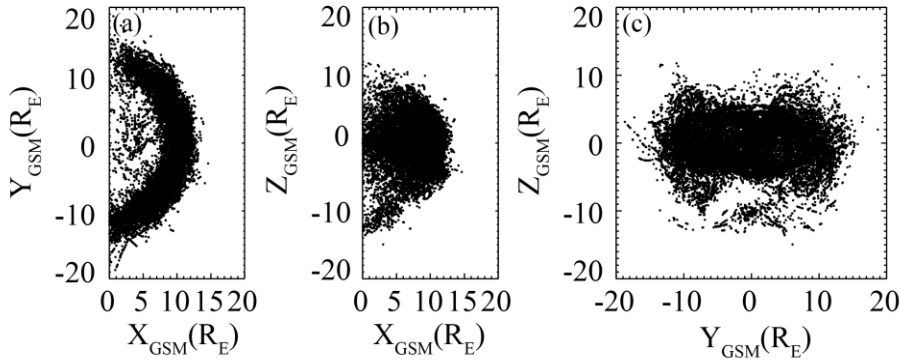
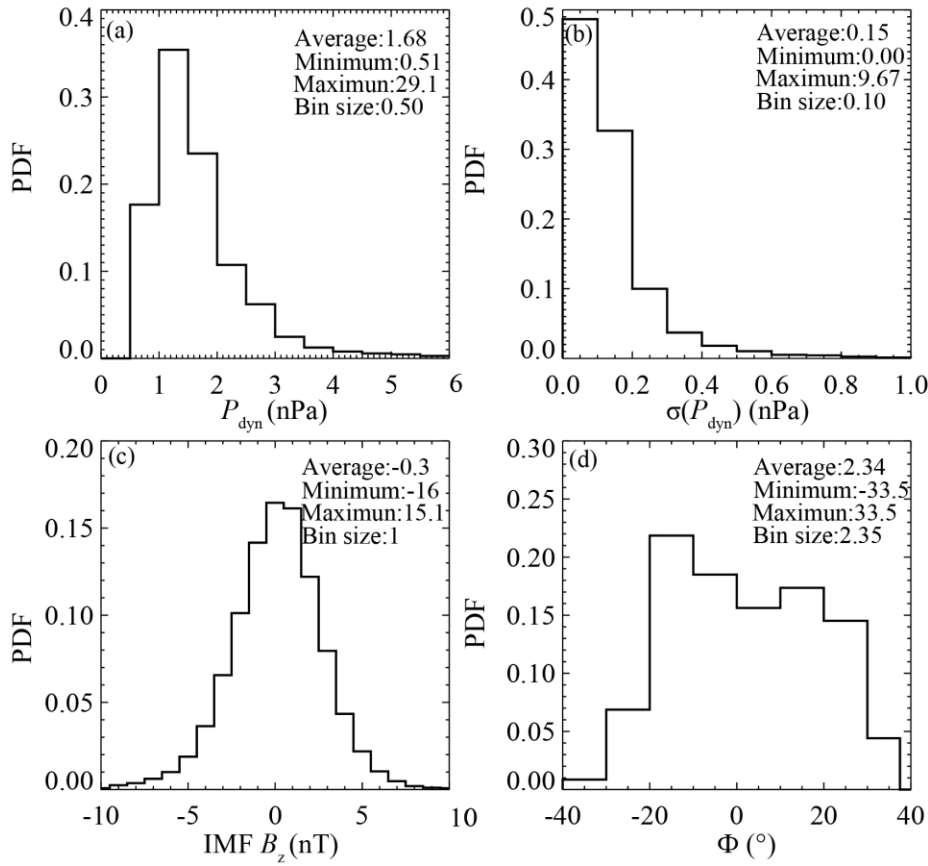


Figure 2: Projections of 38,887 MCEs in GSM coordinate (a) X-Y plane, (b) X-Z plane, (c) Y-Z plane.

143 In previous research on time-independent magnetopause models, the physical models (Ferraro, 1952; Beard, 1960; Spreiter
 144 et al., 1966), although theoretically grounded, usually oversimplify intricate solar wind-magnetosphere interactions to
 145 facilitate calculations, usually without demonstrating apparent higher prediction accuracy compared to widely-used
 146 empirical models (Petrinec and Russell, 1996; Shue et al., 1997; Shue et al., 1998; Chao et al., 2002; Lin et al., 2010)..
 147 Hence, this article concentrates on comparing several notable time-independent empirical models renowned for their
 148 superior prediction accuracy (Petrinec and Russell, 1996; Shue et al., 1997; Shue et al., 1998; Chao et al., 2002; Lin et al.,
 149 2010).



150
 151 **Figure 3: Probability density function of the upstream solar wind observation in (a) solar wind dynamic pressure P_{dyn} , (b)**
 152 **standard deviation of dynamic pressure (P_{dyn}), (c) interplanetary magnetic field B_z component (IMF B_z) and (d) dipole tilt angle**
 153 **(Φ).**

154 Empirical models are typically constructed using satellite observations of MCEs. While these models vary in their use of
 155 satellite datasets, parameters considered, coordinate systems employed, and functions applied, most are parameterized
 156 using the dynamic pressure (P_{dyn}) and the interplanetary magnetic field B_z component (IMF B_z). For example, Petrinec and
 157 Russell (1996) (hereafter PR96) employed an ellipsoidal function to construct a magnetopause model, while Shue et al.

(1997) (hereafter S97) developed a flexible function incorporating two variables: the subsolar magnetopause position (R_0) and the tail flaring angle (α). This function has gained widespread use as a foundational approach to describing magnetopause shape. For instance, Shue et al. (1998) (hereafter S98) accounted for the saturation effect of IMF B_z on R_0 , and Chao et al. (2002) (hereafter C02) extended their model for application under normal and extreme solar wind conditions. Nevertheless, these models primarily rely on low-latitude satellite observations and may not adequately capture the distinctive characteristics of the magnetopause in the higher latitude region. Besides, they are constructed with P_{dyn} and IMF B_z , while it is found that the dipole tilt angle Φ is of great significance in modelling magnetopause, especially in the higher latitude region. Formisano et al. (1979) constructed an average magnetopause size and shape for two dipole tilt angle values (Φ). Boardsen et al. (2000) developed a higher latitude magnetopause model parameterized by not only P_{dyn} and IMF B_z but also the dipole tilt angle (Φ), recognizing its significant influence on the shape of the higher latitude magnetopause. While this model is specifically designed for higher latitude regions, it is not as effective in accurately calculating the magnetopause at low latitudes compared to other models due to inherent limitations.

Table 2 Summary of five widely used magnetopause models and POS model

Model Name	Number of (higher latitude) MCEs used	Time range of MCEs used	Dimensions
PR96	1,147	1979-1980	2D/2.5D
S97	553	1978-1986	2D/2.5D
S98	553	1978-1986	2D/2.5D
C02	552	1978-1986	2D/2.5D
L10	1,226 (1,482)	1994-2008	3D
POS	31,562 (7,325)	2004-2022	3D

The above models are generally developed under the assumption of axial symmetry, while the actual magnetopause shape is asymmetric in both the Y and Z directions, so they are essentially 2D or 2.5D models. To describe the 3D structure of the magnetopause, Lin et al. (2010) (hereafter L10) developed a three-dimensional magnetopause model parameterized by P_{dyn} , thermal pressure (P_t), IMF B_z , and Φ . The coordinate systems employed in these empirical models are typically in aberrated coordinates which accounts for Earth's orbital motion (Petrinec and Russell, 1996; Shue et al., 1997; Shue et al., 1998; Chao et al., 2002), or the corrected coordinates which compensates for both Earth's orbital motion and deviations in solar wind velocity from the Sun-Earth line (Boardsen et al., 2000; Lin et al., 2010). A summary of the five widely used magnetopause models is presented in Table 2.

3 The POS Model

In our previous work (Gu et al., 2023), we modelled the compression-recovery process of the magnetopause as a quasi-elastodynamic phenomenon. In this framework, the dynamic pressure, $\mathbf{P}_{\text{dyn}} = n_{\text{sw}} m_p \mathbf{v}_x^2$, serves as the driving force on the system, where n_{sw} , m_p , and \mathbf{v}_x are the number density, proton mass, and the x component of the solar wind velocity in the GSM coordinates, respectively. The system's restoring force is described by $\mathbf{P}_b = \mathbf{B}^2 / 2\mu_0$, where \mathbf{B} is the total magnetic field at magnetopause and μ_0 is the vacuum permeability. After accounting for damping and non-ideal effects, \mathbf{P}_{damp} , meanwhile neglecting the complex coupling interactions, the momentum equation for the magnetosheath in a unit cylinder can be represented by Eq. (1).

$$M_{\text{msh}} \mathbf{a}_{\text{msh}} = \mathbf{P}_b - \mathbf{P}_{\text{dyn}} - \mathbf{P}_{\text{damp}} \quad (1)$$

Given that the derivation process of the foundational formula is the same as our previous work, and this paper is focused on model predictions rather than physical processes, we will refrain from reiterating it here. The relationship depicting the temporal evolution of the magnetopause position (r) is introduced in Eq. (2).

$$n_{\text{sw}} m_p \mathbf{r} \ddot{\mathbf{r}} = \frac{(\lambda \mathbf{B}_d(\mathbf{r}, \theta, \varphi) + \mathbf{B}_c(\mathbf{r}))^2}{2\mu_0} - n_{\text{sw}} m_p \mathbf{v}_x^2 \cos^2 \alpha - k \Sigma_p \mathbf{B}_p^2 \dot{\mathbf{r}} - \eta \dot{\mathbf{r}} / r \quad (2)$$

Where (r, θ, φ) represents the corresponding spherical coordinates, r is the radial distance, θ is the latitude angle between $[-90^\circ, 90^\circ]$ and φ is the longitude angle adjusted to $[-180^\circ, 180^\circ]$ with 0° oriented towards the Sun for simplicity, and all the vectors have been projected to the normal direction of magnetopause (Gu, et al. 2023). This simplified equation enables us to capture the fundamental dynamics of the magnetopause's response to solar wind fluctuations while ensuring computational efficiency. The first term on the right side of Eq. (2) signifies the restoring force \mathbf{P}_b . Here, \mathbf{B}_d denotes the Earth's dipole field, λ is the magnetospheric compressibility coefficient, and \mathbf{B}_c accounts for contributions from various magnetospheric currents. The second term on the right side represents the driving force \mathbf{P}_{dyn} , where α denotes the angle between the x-direction and the normal direction of the magnetopause. The third term on the right side of Eq. (2) characterizes a position-dependent dragging effect estimated from the ionosphere, while the fourth term illustrates a global non-ideal viscous effect. \mathbf{B}_p is the estimated ionospheric magnetic field in the polar region, Σ_p stands for the equivalent Pederson conductivity, k serves as a position-dependent mapping factor, and η represents the viscous coefficient. The final two terms contribute to the damping and non-ideal effects of the system, denoted as \mathbf{P}_{damp} . Equation (2) provides a foundation for developing a time-dependent magnetopause model that can reflect the system's dynamic behaviour more

205 accurately compared to conventional time-independent models. We will introduce the key parameters in detail in the
206 following sections. All the parameters are in SI units.

207 In this study, we incorporate the impact of IMF B_z and Φ in the magnetospheric magnetic pressure. To determine
208 the equation's final fitting coefficients, we conducted 1,000 independent iterations, each involving a random selection of
209 5,000 MCEs from our dataset of 38,887 MCEs.

210 3.1 The magnetospheric compressibility coefficient (λ)

211 The magnetospheric compressibility coefficient, λ , measures the magnetosphere's response to solar wind pressure,
212 specifically the ratio of the magnetospheric magnetic field to the pure dipolar magnetic field (Spreiter et al., 1966; Schield,
213 1969). This coefficient is one of the most critical parameters directly affecting the position of the magnetopause. Typically,
214 λ has a value of 2.44 at the subsolar point, but it changes as the magnetopause shifts and varies with latitude and longitude,
215 suggesting a more complex formulation (Shue et al., 2011; Chen et al., 2023). Mead and Beard (1964) used a self-
216 consistent method and discovered an inward concave structure at the higher latitude magnetopause, which is influenced by
217 the inclination angle of the Earth's dipole. Their work also determined the surface shape of the magnetopause when the
218 solar wind flow is perpendicular to the dipole axis ($\Phi = 0^\circ$), providing an expression for λ as a function of the angles θ and
219 φ .

220 Several models (Formisano et al., 1979; Boardsen et al., 2000; Lin et al., 2010) have been developed to investigate the
221 influence of Φ (the angle between Earth's magnetic axis and the solar wind direction) on the magnetopause's position and
222 shape, offering valuable insights into the magnetosphere's three-dimensional structure. These models predict an asymmetric
223 response of the magnetosphere to variations in Φ . Boardsen et al. (2000) quantified the effects of Φ on the higher latitude
224 magnetopause using MCEs data from the northern hemisphere. Their work revealed how the dipole tilt angle influences
225 the magnetopause structure in polar regions, which are particularly sensitive to changes in the orientation of Earth's
226 magnetic field relative to the solar wind. Lin et al. (2010) further demonstrated that an increase in Φ causes a slight shift
227 in the centres of the magnetopause cross-sections, moving them towards the negative Z direction in the subsolar region and
228 towards the positive Z direction in the tail region. According to Olson (1969), who provided a detailed representation of λ
229 for various tilt angles ($\Phi = 0^\circ, 10^\circ, 20^\circ, 30^\circ$) on a $15^\circ \times 15^\circ$ grid of θ and φ values, the dipole tilt angle significantly alters
230 the fundamental behaviour of λ , with varying effects on θ and φ . This influence is more pronounced in higher latitude

regions ($\theta > 30^\circ$). Building on previous work by Gu et al. (2023), in which $\lambda = 2.44 - 0.4\theta^2 + \varphi^2$, we incorporate the effect of Φ at different positions of the magnetopause $\lambda(\theta, \varphi)$ and derive a more precise expression for λ , specifically tailored to our model, as presented in Eq. (3):

$$A = \tanh[5.568(|\theta| - 0.5325)] + 1.0$$

$$\lambda(\theta, \varphi, \Phi) = 2.44 - (0.4 + 0.3A)(\theta + 0.2A\Phi)^2 + (1.0 - 0.5A|\Phi|)\varphi^2 \quad (3)$$

3.2 Contributions from various magnetospheric currents (B_c)

Previous studies on the impact of magnetospheric currents on the position of the magnetopause led to the development of a static magnetopause current model, where the magnetic field of magnetopause surface current and tail current were fitted using polynomials to reveal the relationship between variations in the magnetospheric magnetic field and changes in magnetopause position, e.g. $B_{\text{surf}}(r, \theta, \varphi)$ and $B_{\text{tail}}(r, \theta, \varphi)$ (Choe and Beard, 1974b, a; Matsuoka et al., 1995). In our earlier study (Gu et al., 2023), the magnetic field of the current system, denoted as $B_{c0}(r)$, did not account for variations in θ and φ . This limitation is addressed in the present study. The fundamental form of $B_{c0}(r, \theta, \varphi)$, incorporating these angular dependencies, is introduced in Eq. (4). The current system exhibits asymmetry effects, consistent with other models such as T96 and T01 (Tsyganenko, 2001; Tsyganenko, 1996). These models also incorporate dawn-dusk asymmetry in the magnetospheric current, reflecting the influence of these angular dependencies.

$$B_{c0}(r) = [-401904 / (\frac{r}{R_E})^4 + 65489 / (\frac{r}{R_E})^3 + 1500 / (\frac{r}{R_E})^2 - 40][1 + 0.4 \sin(2\theta)^2][1.0 - 0.1 \sin(\varphi)] \times 10^{-9} \quad (4)$$

In our previous work, $B_c(r)$ was defined as a piecewise function of P_{dyn} , which could yield discontinuous and non-physical results at the transition points (Gu et al., 2023). To address this limitation, we now consider the impact of P_{dyn} in a continuous form, eliminating the piecewise dependence. Furthermore, the impact of the IMF B_z on the magnetopause position is directionally dependent, with a southward IMF triggering dayside magnetic reconnection, an essential process already incorporated in most existing models (Aubry et al., 1970; Dungey, 1961; Fairfield, 1971). To quantify this effect, we adopt a hyperbolic tangent function, similar to that in Shue et al. (1998). Finally, by considering the combined effects of both IMF B_z and P_{dyn} , B_c is expressed as in Eq. (5):

$$B_c = B_{c0}(r, \theta, \varphi) f(B_z) f(P_{\text{dyn}})$$

$$= B_{c0}(r) [1.0 + 0.2 \tanh(-0.5(B_z + 2.5))][1 + 0.1 P_{\text{dyn}}] \quad (5)$$

254 This formulation of \mathbf{B}_c provides a more refined and physically accurate depiction of the influence of the magnetospheric
 255 current system on magnetopause dynamics. By incorporating the dependence of \mathbf{B}_c on IMF \mathbf{B}_z and \mathbf{P}_{dyn} and specific
 256 locations on the magnetopause, the expression captures the complex spatial variations in the magnetospheric current system
 257 that contribute to magnetic pressure, making our model fully three-dimensional.

258 3.3 The damping items

259 The damping terms in our model consist of a position-dependent dragging effect from the ionosphere $\mathbf{F}_d = k \Sigma_p \mathbf{B}_p^2 \dot{\mathbf{r}}_{\text{mp}}$
 260 and a global non-ideal viscous effect $\mathbf{F}_N = \eta \dot{\mathbf{r}}_{\text{mp}} / \mathbf{r}_{\text{mp}}$, consistent with our previous work (Chen and Wolf, 1999; Wang
 261 and Chen, 2008; Gu et al., 2023). We set $\mathbf{B}_p = 3 \times 10^{-5}$ T to represent the approximate ionospheric magnetic field in the polar
 262 region, while $\Sigma_p = 3.4$ S serves as the equivalent Pedersen conductivity. The viscous coefficient is artificially set to $\eta = 2 \times 10^{-8}$.
 263 As defined in Eq. (6), the position-dependent mapping factor k is empirically calibrated based on the magnetopause
 264 location (r, θ, φ) , increasing when the magnetopause compresses and decreasing with increasing latitude and longitude.

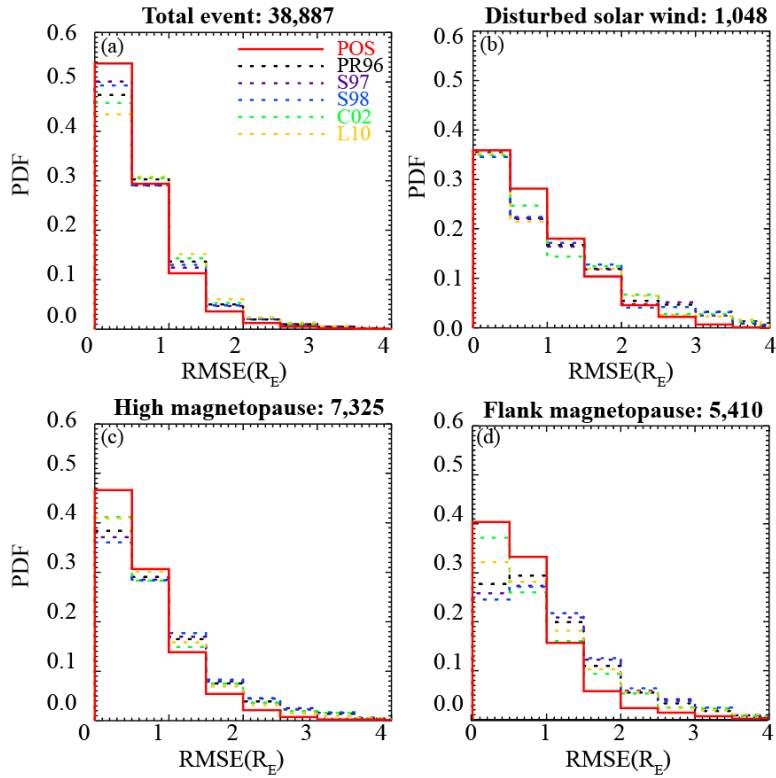
$$265 \quad k = [196(0.05 + e^{-0.05(r/R_E)^2}) - 3.2|\theta| - 1.6|\varphi|] \times 10^{-7} \quad (6)$$

266 4 Result

267 By substituting the relevant parameters into Eq. (2) and assuming the initial shape of the magnetopause as a paraboloid,
 268 $x = -0.03(y^2 + z^2) + R_0$, where R_0 is determined by the pressure balance at the subsolar point, the position of each point on the
 269 magnetopause can be computed instantaneously on a personal computer. The prediction accuracy of the POS model and
 270 other notable time-independent models mentioned earlier is evaluated and compared with MCEs at the real THEMIS
 271 location. We use the root-mean-square error (RMSE), denoted as Δ , to quantify the prediction accuracy by comparing the
 272 model's calculations with MCE observations. A dataset of 38,887 MCEs observed by the THEMIS and CLUSTER satellites
 273 is used for testing. To evaluate the performance of the POS model relative to other models, we calculate the ratio $\delta(\Delta)/\Delta_{\text{POS}}$,
 274 where $\delta(\Delta)$ represents the difference in RMSE between a previous model and the POS model, and Δ_{POS} is the RMSE of the
 275 POS model. This comparison is conducted from various perspectives. The probability density distributions of RMSE for
 276 each model are illustrated in Figure 4.

277 It can be seen that all models are capable of adequately predicting magnetopause positions, with the majority ($> 70\%$)
 278 showing RMSE within 1 R_E . Our model demonstrates superior accuracy, with 80% of its prediction errors falling below 1

279 R_E . Predicting the magnetopause under disturbed solar wind conditions is more challenging, while the POS model shows
 280 improved performance in such conditions, with 60% of predictions remaining within 1 R_E . Given the inherent asymmetry
 281 of the magnetopause, we evaluated the models' performance in both the flank region ($|\phi| \geq 60^\circ$) and the higher latitude
 282 region ($|\theta| \geq 30^\circ$). The POS model consistently outperforms the others in both regions, especially in the flank region.
 283 Notably, as a time-dependent three-dimensional model, the POS model seldom produces poor predictions, with RMSE
 284 exceeding 3 R_E in only rare cases.



285
 286 **Figure 4:** Distribution of models' RMSE in total(a) and in disturbed solar wind(b); (c) and (d) is the prediction ability in higher
 287 latitude magnetopause ($|\theta| \geq 30^\circ$) and in magnetopause flank region ($|\phi| \geq 60^\circ$)

288 4.1 Time-dependent feature

289 The models' prediction accuracy is listed in Table 3, it can be seen that all evaluated models exhibit remarkable predictive
 290 capabilities, with $\Delta < 1 R_E$, aligning closely with other statistical results found in the literature (Staples et al., 2020b). While
 291 it should be noted that the Δ values calculated for other models in this study may slightly differ from those reported in their
 292 original papers. This discrepancy arises due to our use of a significantly larger MCE dataset for comparison.

293

294

295 **Table 3 Models' prediction accuracy for all MCEs and in disturbed solar wind.**

Model Name	Total (38,887 MCEs)		[$\sigma(\mathbf{P}_{\text{dyn}})/\langle \mathbf{P}_{\text{dyn}} \rangle$] > 100% (1,048 MCEs)	
	$\Delta(\mathbf{R}_E)$	$\delta(\Delta) / \Delta_{\text{POS}}$	$\Delta(\mathbf{R}_E)$	$\delta(\Delta) / \Delta_{\text{POS}}$
PR96	0.899	+16.1%	1.389	+23.6%
S97	0.884	+14.2%	1.383	+23.0%
S98	0.894	+15.5%	1.388	+23.5%
C02	0.926	+19.6%	1.325	+17.9%
L10	0.960	+24.0%	1.377	+22.5%
POS	0.774	Average:17.9%	1.124	Average:22.1%

296 Notably, the POS model demonstrates superior predictive performance, with an average improvement of 17.9% over the
 297 other models. Additionally, time-independent models have inherent limitations in capturing the dynamic response of the
 298 magnetosphere to solar wind fluctuations, particularly when the magnetopause standoff distance is not in phase with \mathbf{P}_{dyn}
 299 (Archer et al., 2019). In cases of highly disturbed upstream solar wind, where the ratio of standard deviation of \mathbf{P}_{dyn} to
 300 average \mathbf{P}_{dyn} ($\sigma(\mathbf{P}_{\text{dyn}})/\langle \mathbf{P}_{\text{dyn}} \rangle$) exceeds 100%, the POS model shows an even greater improvement in predictive accuracy,
 301 with a 22.1% enhancement compared to other models. These results suggest that by incorporating time-dependent effects
 302 into magnetopause modelling, particularly during periods of solar wind disturbance, the POS model can more effectively
 303 capture the non-linear and out-of-phase responses of the magnetopause to rapidly changing solar wind conditions. These
 304 results also indicate that time-dependent model represents an obvious advancement in predicting and understanding
 305 magnetospheric dynamics across a wide range of solar wind conditions.

306 The magnetopause is rarely static, exhibiting continuous motion under varying solar wind conditions and displaying
 307 complex dynamics during both intense disturbances and gentle changes. A notable feature of these dynamics is the periodic
 308 oscillation within the Pc5 frequency range (2-7 mHz), often termed the “magic frequency” in magnetospheric physics
 309 (Samson et al., 1992; Plaschke et al., 2009a; Plaschke et al., 2009b). The magnetopause oscillations can be driven by quasi-
 310 periodic solar wind dynamic fluctuations or explained by magnetospheric cavity mode and Kruskal-Schwarzschild mode
 311 (Archer et al., 2013; Kruskal and Schwarzschild, 1954; Kepko and Spence, 2003; Kivelson et al., 1984). Our previous
 312 research indicates that the oscillations of the magnetopause ought to have eigenfrequencies (f_0) which are determined by
 313 the restoring force (\mathbf{P}_B), the external driving force (\mathbf{P}_{dyn}) as well as the damping force (\mathbf{P}_{damp}) (David Halliday, 2021;
 314 Freeman et al., 1995; Gu et al., 2023). Magnetopause will respond to solar wind with phase difference ranging from 0 to

315 180 degrees, depending on the driving frequency of the solar wind (f_{drive}). The magnetopause behaves as a low-pass filter,
 316 effectively screening out very high-frequency solar wind fluctuations (e.g., $f_{\text{drive}} > 15f_0$, where f_0 is the eigenfrequency of the
 317 magnetopause). The magnetopause behaves as a low-pass filter, effectively screening out very high-frequency solar wind
 318 fluctuations (e.g., $f_{\text{drive}} > 15f_0$, where f_0 is the eigenfrequency of the magnetopause). This filtering effect results in smoother
 319 predictions of magnetopause behaviour, **which can** be found in Figure 5. For relatively high fluctuations (e.g., $15f_0 >$
 320 $f_{\text{drive}} > 2f_0$), the phase difference between the solar wind and magnetopause approaches 180 degrees, indicating an anti-phase
 321 response. At resonance ($f_{\text{drive}} \approx f_0$), the magnetopause exhibits a 90-degree phase lag relative to the solar wind forcing.
 322 Conversely, the magnetopause only behaves in-phase with the solar wind under low-frequency fluctuations ($f_{\text{drive}} < 0.5f_0$),
 323 which is the scenario typically revealed by time-independent models.
 324 The time-dependent POS model demonstrates the capability to depict these magnetosphere oscillations and the phase
 325 difference accurately. Figure 5 presents two specific cases illustrating the POS model's time-dependent performance
 326 compared with subsolar MCEs projected from THEMIS. In Case I, both models initially predict the magnetopause position
 327 at $\sim 11.5 R_E$ before a pressure pulse in solar wind. The POS model uniquely predicts four oscillations around its equilibrium
 328 position ($\sim 10 R_E$) before the magnetopause reaches a new pressure balance. This dynamic behaviour cannot be physically
 329 captured by any time-independent models. In Case II, the POS model accurately captures the oscillations around 21:24
 330 UT-21:33 UT, which are not all in-phase with the solar wind dynamic pressure (P_{dyn}). Notably, the POS model depicts
 331 anti-phase responses observed in the second and third crossings, while the S98 model shows a reverse trend in motion that
 332 deviates more from observations. These results suggest that by incorporating time-dependent effects into magnetopause
 333 modelling, particularly during periods of solar wind disturbance, the POS model can more effectively capture the non-
 334 linear and out-of-phase responses of the magnetopause to rapidly changing solar wind conditions.

335

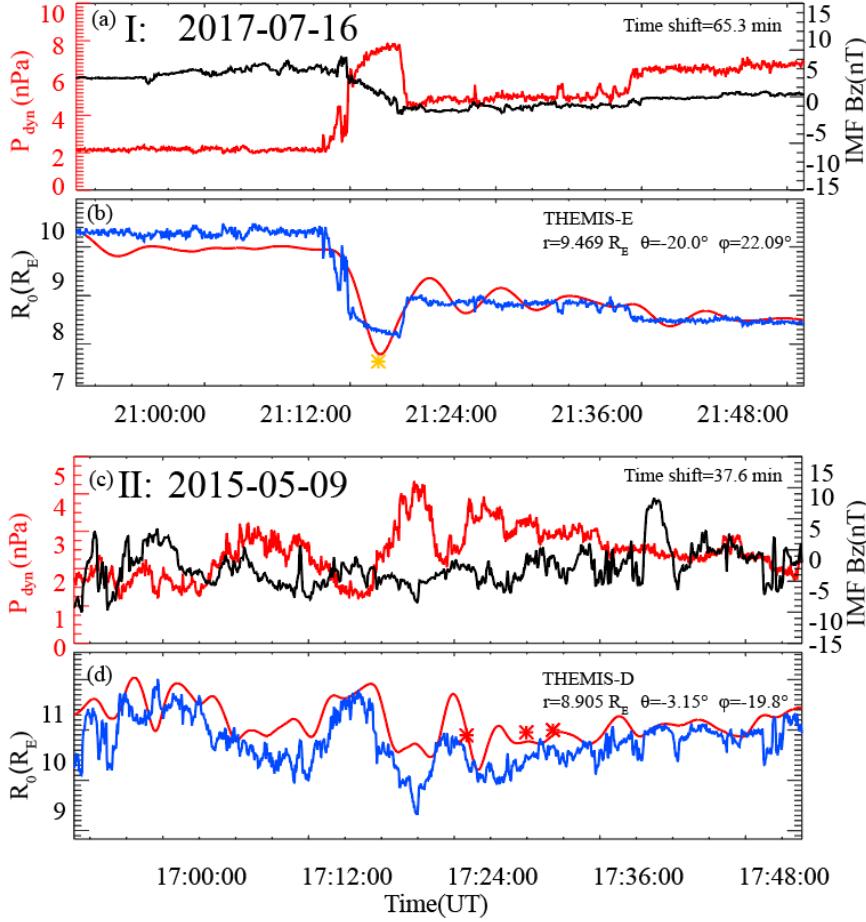


Figure 5: Case study for the overall oscillation of magnetopause using time-independent model S98 and time-dependent POS model to predict its position. (a), (c) The corresponding upstream solar wind dynamic pressure P_{dyn} (red line) and interplanetary magnetic field B_z component (black line) observed by Wind with a time shift of 65.3 min and 37.6 min, respectively; (b), (d) The predictions of S98 (blue) and POS (red) model's prediction based the input solar wind and the asterisks represent the subsolar positions of MCEs projected from THEMIS.

4.2 Three-dimensional characteristic

The POS model developed here incorporates the asymmetrical effects of dipole tilt angles, latitude, and longitude differences, as integrated into Eq. (2) and (3). The model's parameters were comprehensively calibrated, allowing it to more accurately depict the three-dimensional shape of the magnetopause. To assess its validity across different magnetopause regions, extensive tests were performed, with results presented in Table 4. In the higher latitude magnetopause ($|\theta| \geq 30^\circ$), a region where many models face challenges, the POS model, alongside the L10 model, demonstrates superior performance, showing an impressive 27.0% improvement in accuracy compared to other models. Similarly, in the flank regions ($|\phi| \geq 60^\circ$), where surface waves and other magnetospheric fluctuations complicate position and shape determination, the POS model maintains its high accuracy, with a 33.3% improvement over other models. These

351 results suggest that the POS model offers a more accurate and comprehensive representation of the magnetopause across
 352 its entire structure, outperforming other models in both higher latitude and flank regions.

353 **Table 4 Models' prediction accuracy for higher latitude and flank regions**

Model name	$ \theta \geq 30^\circ$ (7,325 MCEs)	$ \phi \geq 60^\circ$ (5,410 MCEs)		
	$\langle \Delta \rangle (R_E)$	$\delta (\Delta) / \Delta_{POS}$	$\Delta (R_E)$	$\delta (\Delta) / \Delta_{POS}$
PR96	1.149	+27.8%	1.315	+31.8%
S97	1.180	+31.3%	1.388	+39.1%
S98	1.195	+32.9%	1.403	+40.6%
C02	1.130	+25.7%	1.268	+27.1%
L10	1.053	+17.1%	1.278	+28.0%
POS	0.899	Average:27.0%	0.998	Average:33.3%

354 Surface waves are a distinct feature of the magnetopause, originating from various factors, including solar wind and bow
 355 shock dynamics, as well as instabilities within the magnetopause and magnetosphere under specific conditions. Several
 356 localized physical processes have been identified as potential drivers of these surface waves, including the Kelvin-
 357 Helmholtz instability, magnetic reconnection and flux transfer event (Hartering et al., 2013; Agapitov et al., 2009; Archer
 358 et al., 2021). It is also found that a tailward-moving surface wavelet could be driven by disturbed solar wind (large σ
 359 $(P_{dyn}) / \langle P_{dyn} \rangle$) (Sibeck et al., 1989). Our previous study revealed a distinct mechanism for the formation of surface wave-
 360 like structures in the magnetopause (Gu et al., 2023). The interplay between dynamic pressure (P_{dyn}), magnetic pressure
 361 (P_b), and damping pressure (P_{damp}) results in different oscillation periods at various points on the magnetopause. These
 362 variations create a time lag within the magnetopause structure, manifesting as a surface wave-like pattern. Figure 6 shows
 363 a surface wave-like structure predicted by the POS model during relatively disturbed upstream solar wind conditions. The
 364 POS model's predictions are compared with those of the C02 model, which has been demonstrated as the most effective
 365 time-independent model in the flank region according to our evaluation. Figure 6 presents a specific case study illustrating
 366 the POS model's time-dependent performance compared with THEMIS MCEs positions mapped to the X-Y plane. Figure
 367 6 (a) displays the solar wind dynamic pressure and the north-south component of the interplanetary magnetic field. The
 368 radial positions of the different points in magnetopause in the XY plane ($Z=0$), as calculated by our model—being fully
 369 three-dimensional—exhibits an asymmetric flank region, are traced in Figure 6(b). Positive and negative flanks respond
 370 differently to variations in the solar wind, with discrepancies becoming more pronounced at higher ϕ . In this specific

example, the dusk region is more significantly disturbed than the dawn region. Notably, the magnetopause shapes calculated in Figure 6(c)-(e) reveal surface wave-like structures evolving over time. THEMIS MCEs observed in the flank region corroborate this predicted surface wave-like structure, indicating that the magnetopause position predicted by the POS model is more accurate than that predicted by the C02 model.

The POS model's predictions are compared with those of the C02 model, which has been demonstrated as the most effective time-independent model in the flank region according to our evaluation. Figure 6 illustrates a surface wave-like structure predicted by the POS model during relatively disturbed upstream solar wind conditions. The predicted surface wave-like structure is corroborated by THEMIS MCEs in the flank region, where the actual magnetopause position is closer to Earth than predicted by C02 model.

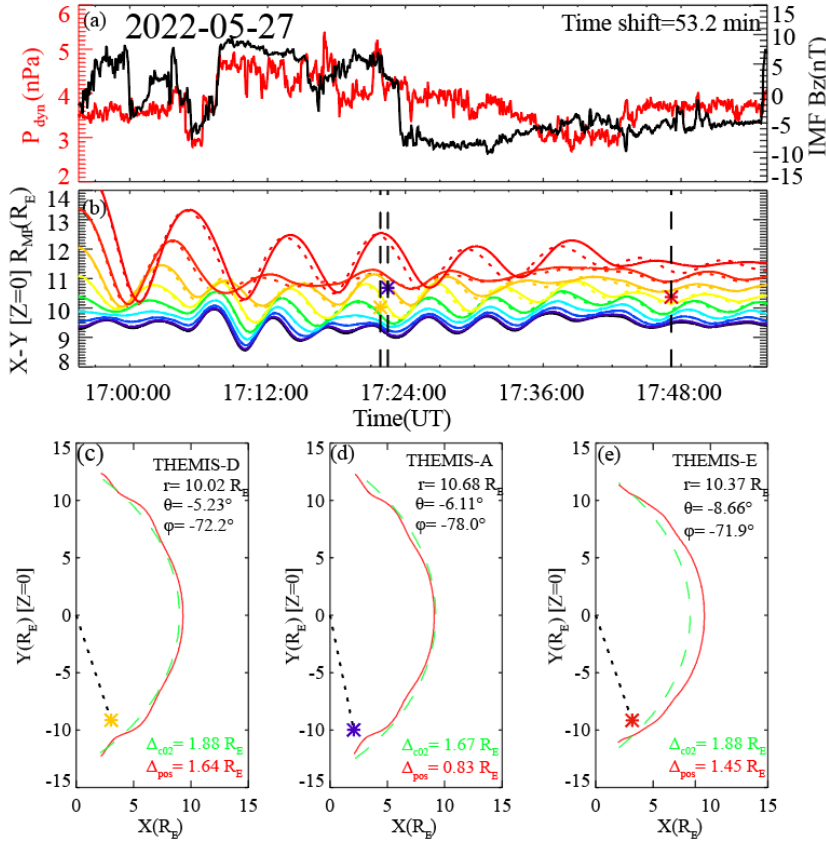


Figure 6: A surface wave-like structure in X-Y magnetopause flank region. (a) The corresponding solar wind dynamic pressure (red) and IMF Bz component (black), (b) The red, orange, yellow, green, blue, purple and black colours represent the initial magnetopause positions at $\phi = \pm 80^\circ$, $\pm 70^\circ$, $\pm 60^\circ$, $\pm 50^\circ$, $\pm 40^\circ$, $\pm 30^\circ$, $\pm 20^\circ$, $\pm 10^\circ$, 0° , respectively (dot line is the corresponding negative value of ϕ). The asterisk in purple (THEMIS-A), yellow (THEMIS-D) and red (THEMIS-E) indicate the satellite observation of MCEs projected onto the X-Y plane; (c) (d) (e) The shape of magnetopause in the X-Y plane at different time predicted by POS model (red dash line) and C02 model (green dot line), the asterisks represent the THEMIS MCEs positions mapped to X-Y plane.

5 Discussion and Conclusion

Accurately calculating the position of the magnetopause is essential for space weather forecasting and understanding the underlying physical mechanisms involved in the solar wind-magnetosphere interaction. In this work, we developed the POS model, the first time-dependent three-dimensional magnetopause model based on quasi-elastodynamic theory. By incorporating key solar wind parameters such as P_{dyn} , IMF B_z and Φ , this model effectively depicts magnetopause dynamics. The POS model offers a new approach to describing magnetopause position, overall oscillation, and surface wave-like structures as interconnected phenomena. Its time-dependent feature excels in capturing dynamic processes, particularly under highly disturbed solar wind conditions. The three-dimensional nature allows for accurate depiction of the overall magnetopause shape, with notable precision in higher latitude regions and flank areas. This capability addresses limitations in existing models and provides a more comprehensive picture of magnetopause dynamics from a different perspective.

However, there are still limitations and areas for improvement that future research should address:

(1) Adapting to extreme solar wind conditions: Similar to the force-deformation relationship of a spring that requires a specific range of applicability, the POS model has not been specifically optimized for extreme solar wind conditions (e.g., $P_{\text{dyn}} < 0.5$ nPa and $P_{\text{dyn}} > 40$ nPa). When the solar wind dynamic pressure is low, the quasi-elastic process between the solar wind and the magnetopause exhibits stronger damping characteristics, while at very high solar wind dynamic pressures, the magnetopause shows increased rigidity. Future iterations could incorporate more suitable damping coefficients and include P_{dyn} in the magnetospheric compressibility coefficient to broaden the model's applicability range.

(2) Incorporating additional solar wind factors: Existing research has shown that even under similar solar wind dynamic pressure conditions, changes in solar wind density and velocity have distinct effects on magnetopause position (Samsonov et al., 2020). Additionally, the influence of solar wind temperature, more comprehensive IMF effects (e.g., B_x and B_y), and other solar wind components (e.g., alpha particles) on magnetopause position are not reflected in the current model. Moreover, magnetosheath transient effects and other perturbations on the magnetopause position are not addressed (Silveira et al., 2024; Silveira and Sibeck, 2023; Sibeck et al., 2022). Future models could consider introducing these factors to achieve better predictive results.

(3) Better nightside extension: The current POS model is primarily based on the dayside quasi-elastodynamic theory and is calibrated and validated using dayside MCEs. In the future, the model's calculation results for the nightside region could

414 be improved by combining the fitting approach of empirical models with a more flexible curve function calibrated using a
 415 larger number of nightside MCE observations.

416 (4) Cusp region representation: Accurately modelling the magnetopause cusp region, shaped by Earth's dipole field,
 417 remains challenging. While some models approximate this region by fitting two distinct curves, capturing its shape and
 418 position precisely is complex. Improving the representation of the cusp region will require further analysis of higher latitude
 419 satellite data to enhance model accuracy.

420 (5) Parameter fine-tuning: Further refinement of model parameters, potentially through machine learning techniques or
 421 implementing piecewise functions for different regions, could improve the model's accuracy. However, as noted in the
 422 introduction, it's important to balance model complexity with practicality. Overly complex parameter expressions can lead
 423 to increased inconvenience and higher computational costs. For those seeking the highest possible prediction accuracy, a
 424 more practical approach might involve using numerical simulations.

425 The upcoming SMILE mission (Solar wind Magnetosphere Ionosphere Link Explorer), a joint mission between the Chinese
 426 Academy of Sciences and the European Space Agency, is set to launch in 2025 (Branduardi-Raymont et al., 2018; Chi and
 427 Graziella, 2018). This mission will provide more detailed data on magnetopause position and polar cap shape over time,
 428 enhancing the ability to validate and refine existing magnetopause models.

429 In summary, this study introduces the POS model, the first time-dependent three-dimensional magnetopause model based
 430 on quasi-elastodynamic theory. Unlike time-independent models, the POS model effectively captures the dynamic
 431 movement of the magnetopause under varying solar wind conditions. When compared to five widely used models, the POS
 432 model demonstrates superior predictive accuracy, showing a 17.9% improvement with $RMSE=0.774 R_E$. As a time-
 433 dependent model, it demonstrated superior accuracy under highly disturbed solar wind conditions (22.1% better). Its three-
 434 dimensional nature allows for enhanced accuracy in higher latitude regions (27.0% better) and flank regions (33.3% better)
 435 of the magnetopause. Moreover, compared to numerical simulations, the POS model offers a concise formulation with
 436 rapid computational speed, making it feasible for direct deployment on satellites in the future, where onboard chips could
 437 complete calculations, greatly enhancing satellite intelligence. By providing a more precise and dynamic representation of
 438 the magnetopause, the POS model enhances our ability to predict and analyse space weather events and may also offer new
 439 insights and methodologies for developing magnetopause models for other planets.

440 **Code and data availability**

441 The current version of model is available from the project website: http://www.spaceweather.org.cn/pos_model. The exact
442 version of the model used to produce the results used in this paper is archived on Zenodo:
443 <https://zenodo.org/records/15162611> . The URL includes the code and the list of MCEs used in this paper. The data of
444 THEMIS satellite can be obtained from <https://cdaweb.gsfc.nasa.gov/pub/data/themis/> , and the data of WIND satellite
445 can be obtained from <https://cdaweb.gsfc.nasa.gov/pub/data/wind/> .

446 **Competing interests**

447 The contact author has declared that none of the authors has any competing interests.

448 **Author contribution**

449 Y. W. designed the model. Y.X.G developed the model code and carried it out. Y. X. G and Y. W. prepared the original
450 manuscript. Y. X. G and X. J. S. prepared the MCE list. F. S. W., X. S. F., A. S., X. J. S., B. Y. W., P. B. Z., C. W. J., Y.
451 L. C, X. J. X., and Z. L. Z. discussed the scientific results, reviewed and revised the manuscript.

452 **Acknowledgements**

453 We thank NASA/GSFC CDAWeb for providing the Wind, THEMIS and Cluster data. This work is jointly supported by
454 the National Key R & D Program of China (Grant No. 2022YFF0503900), National Natural Science Foundation of China
455 42174199 and 42030204, China Scholarship Council 202306120305, Guangdong Basic and Applied Basic Research
456 Foundation 2023B1515040021, and Shenzhen Technology Project JCYJ20210324121210027, RCJC20210609104422048,
457 GXWD20220817152453003, and Shenzhen Key Laboratory Launching Project No. ZDSYS20210702140800001.

References

- Agapitov, O., Glassmeier, K.-H., Plaschke, F., Auster, H.-U., Constantinescu, D., Angelopoulos, V., Magnes, W., Nakamura, R., Carlson, C. W., Frey, S., and McFadden, J. P.: Surface waves and field line resonances: A THEMIS case study, *Journal of Geophysical Research: Space Physics*, 114, A00C27, 10.1029/2008ja013553, 2009.
- Ala-Lahti, M., Pulkkinen, T. I., Pfau-Kempf, Y., Grandin, M., and Palmroth, M.: Energy Flux Through the Magnetopause During Flux Transfer Events in Hybrid-Vlasov 2D Simulations, *Geophysical Research Letters*, 49, 10.1029/2022gl100079, 2022.
- Anderson, K. A., Binsack, J. H., and Fairfield, D. H.: HYDROMAGNETIC DISTURBANCES OF 3- TO 15-MINUTE PERIOD ON MAGNETOPAUSE AND THEIR RELATION TO BOW SHOCK SPIKES, *Journal of Geophysical Research*, 73, 2371-2386, 10.1029/JA073i007p02371, 1968.
- Angelopoulos, V.: The THEMIS mission, *Space Science Reviews*, 141, 5-34, 10.1007/s11214-008-9336-1, 2008.
- Archer, M. O., Hartinger, M. D., and Horbury, T. S.: Magnetospheric “magic” frequencies as magnetopause surface eigenmodes, 40, 5003-5008, <https://doi.org/10.1002/grl.50979>, 2013.
- Archer, M. O., Hartinger, M. D., Plaschke, F., Southwood, D. J., and Rastaetter, L.: Magnetopause ripples going against the flow form azimuthally stationary surface waves, *Nature Communications*, 12, 10.1038/s41467-021-25923-7, 2021.
- Archer, M. O., Hietala, H., Hartinger, M. D., Plaschke, F., and Angelopoulos, V.: Direct observations of a surface eigenmode of the dayside magnetopause, *Nature Communications*, 10, 10.1038/s41467-018-08134-5, 2019.
- Ashida, Y., Yamakawa, H., Funaki, I., Usui, H., Kajimura, Y., and Kojima, H.: Thrust Evaluation of Small-Scale Magnetic Sail Spacecraft by Three-Dimensional Particle-in-Cell Simulation, *Journal of Propulsion and Power*, 30, 186-196, 10.2514/1.B35026, 2014.
- Aubry, M. P., Russell, C. T., and Kivelson, M. G. J. J. o. G. R.: Inward motion of the magnetopause before a substorm, 75, 7018-7031, 1970.
- Auster, H. U., Glassmeier, K. H., Magnes, W., Aydogar, O., Baumjohann, W., Constantinescu, D., Fischer, D., Fornacon, K. H., Georgescu, E., Harvey, P., Hillenmaier, O., Kroth, R., Ludlam, M., Narita, Y., Nakamura, R., Okrafka, K., Plaschke, F., Richter, I., Schwarzl, H., Stoll, B., Valavanoglou, A., and Wiedemann, M.: The THEMIS Fluxgate Magnetometer, *Space Science Reviews*, 141, 235-264, 10.1007/s11214-008-9365-9, 2008.
- Balogh, A., Dunlop, M. W., Cowley, S. W. H., Southwood, D. J., Thomlinson, J. G., Glassmeier, K. H., Musmann, G., Lühr, H., Buchert, S., Acuña, M. H., Fairfield, D. H., Slavin, J. A., Riedler, W., Schwingenschuh, K., and Kivelson, M. G.: The Cluster Magnetic Field Investigation, in: *The Cluster and Phoenix Missions*, edited by: Escoubet, C. P., Russell, C. T., and Schmidt, R., Springer Netherlands, Dordrecht, 65-91, 10.1007/978-94-011-5666-0_3, 1997.
- Beard, D. B.: The interaction of the terrestrial magnetic field with the solar corpuscular radiation, 65, 3559-3568, <https://doi.org/10.1029/JZ065i011p03559>, 1960.

- 490 Boardsen, S. A., Eastman, T. E., Sotirelis, T., and Green, J. L.: An empirical model of the high-latitude magnetopause, 105, 23193-23219, <https://doi.org/10.1029/1998JA000143>, 2000.
- Borovsky, J. E. and Alejandro Valdivia, J.: The Earth's Magnetosphere: A Systems Science Overview and Assessment, *Surveys in Geophysics*, 39, 817-859, 10.1007/s10712-018-9487-x, 2018.
- Børve, S., Sato, H., Pécseli, H., and Trulsen, J.: Minute-scale period oscillations of the magnetosphere, *Annales Geophysicae*, 495 29, 663-671, 10.5194/angeo-29-663-2011, 2011.
- Branduardi-Raymont, G., Wang, C., Escoubet, C. P., Adamovic, M., Agnolon, D., Berthomier, M., Carter, J. A., Chen, W., Colangeli, L., Collier, M., Connor, H. K., Dai, L., Dimmock, A., Djazovski, O., Donovan, E., Eastwood, J. P., Enno, G., Giannini, F., Huang, L., Kataria, D., Kuntz, K., Laakso, H., Li, J., Li, L., Lui, T., Loicq, J., Masson, A., Manuel, J., Parmar, A., Piekutowski, T., Read, A. M., Samsonov, A., Sembay, S., Raab, W., Ruciman, C., Shi, J. K., Sibeck, D. G., Spanswick, E. 500 L., Sun, T., Symonds, K., Tong, J., Walsh, B., Wei, F., Zhao, D., Zheng, J., Zhu, X., and Zhu, Z.: SMILE Definition Study Report, European Space Agency, Esa/sci, 1, 2018.
- Chao, J. K., Wu, D., Lin, C. H., Yang, Y. H., Wang, X. Y., Kessel, M., Chen, S. H., and Lepping, R. P.: Models for the size and shape of the Earth's magnetopause and bow shock, *COSPAR Colloquia Series*, 12, 127-135, 10.1016/S0964-2749(02)80212-8, 2002.
- 505 Chapman, S. and Ferraro, V. C. A.: A New Theory of Magnetic Storms, *Journal of Geophysical Research*, 38, 79-96, 10.1038/126129a0, 1930.
- Chen, C. X. and Wolf, R. A.: Theory of thin-filament motion in Earth's magnetotail and its application to bursty bulk flows, *Journal of Geophysical Research-Space Physics*, 104, 14613-14626, 10.1029/1999ja900005, 1999.
- Chen, Y.-W., Shue, J.-H., Zhong, J., and Shen, H.-W.: Anomalous Response of Mercury's Magnetosphere to Solar Wind 510 Compression: Comparison to Earth, *The Astrophysical Journal*, 957, 26, 10.3847/1538-4357/acf655, 2023.
- Chi, W. and Graziella, B. R.: Progress of Solar Wind Magnetosphere Ionosphere Link Explorer (SMILE) Mission, *空间科学学报*, 38, 657-661, 2018.
- Choe, J. Y. and Beard, D. B.: The compressed geomagnetic field as a function of dipole tilt, *Planetary and Space Science*, 22, 595-608, [https://doi.org/10.1016/0032-0633\(74\)90093-2](https://doi.org/10.1016/0032-0633(74)90093-2), 1974a.
- 515 Choe, J. Y. and Beard, D. B.: The near earth magnetic field of the magnetotail current, *Planetary and Space Science*, 22, 609-615, [https://doi.org/10.1016/0032-0633\(74\)90094-4](https://doi.org/10.1016/0032-0633(74)90094-4), 1974b.
- Collado-Vega, Y. M., Dredger, P., Lopez, R. E., Khurana, S., Rastaetter, L., Sibeck, D., and Anastopulos, M.: Magnetopause Standoff Position Changes and Geosynchronous Orbit Crossings: Models and Observations, *Space Weather*, 21, e2022SW003212, <https://doi.org/10.1029/2022SW003212>, 2023.
- 520 David Halliday, R. R., Jearl Walker: *Fundamentals of Physics, Extended*, 12th Edition, in: *Fundamentals of Physics, Extended*, 12th Edition, Wiley, 456-458, 2021.

- Desai, R. T., Freeman, M. P., Eastwood, J. P., Eggington, J. W. B., Archer, M. O., Shprits, Y. Y., Meredith, N. P., Staples, F. A., Rae, I. J., Hietala, H., Mejnertsen, L., Chittenden, J. P., and Horne, R. B.: Interplanetary Shock-Induced Magnetopause Motion: Comparison Between Theory and Global Magnetohydrodynamic Simulations, *Geophysical Research Letters*, 48, 10.1029/2021gl092554, 2021.
- Dungey, J. W.: Interplanetary Magnetic Field and the Auroral Zones, *Physical Review Letters*, 6, 47-48, 10.1103/PhysRevLett.6.47, 1961.
- Eastwood, J. P., Hietala, H., Toth, G., Phan, T. D., and Fujimoto, M.: What Controls the Structure and Dynamics of Earth's Magnetosphere?, *Space Science Reviews*, 188, 251-286, 10.1007/s11214-014-0050-x, 2015.
- Escoubet, C. P., Fehringer, M., and Goldstein, M.: The Cluster mission - Introduction, *Annales Geophysicae*, 19, 1197-1200, 10.5194/angeo-19-1197-2001, 2001.
- Fairfield, D. H.: Average and unusual locations of the Earth's magnetopause and bow shock, 76, 6700-6716, <https://doi.org/10.1029/JA076i028p06700>, 1971.
- Feng, X.: Current Status of MHD Simulations for Space Weather, in: *Magnetohydrodynamic Modeling of the Solar Corona and Heliosphere*, edited by: Feng, X., Springer Singapore, Singapore, 1-123, 10.1007/978-981-13-9081-4_1, 2020.
- Ferraro, V. C. A.: On the theory of the first phase of a geomagnetic storm: A new illustrative calculation based on an idealised (plane not cylindrical) model field distribution, 57, 15-49, <https://doi.org/10.1029/JZ057i001p00015>, 1952.
- Formisano, V., Domingo, V., and Wenzel, K.-P.: The three-dimensional shape of the magnetopause, *Planetary and Space Science*, 27, 1137-1149, 10.1016/0032-0633(79)90134-x, 1979.
- Freeman, M. P. and Farrugia, C. J.: Magnetopause motions in a Newton-Busemann approach, *Nato Adv Sci I C-Mat*, 509, 15-26, 1998.
- Freeman, M. P., Freeman, N. C., and Farrugia, C. J.: A Linear Perturbation Analysis of Magnetopause Motion in the Newton-Busemann Limit, *Ann Geophys*, 13, 907-918, DOI 10.1007/s005850050230, 1995.
- Gargaté, L., Fonseca, R. A., Bingham, R., and Silva, L. O.: Expansion of a plasma cloud into the solar wind, *Ieee Transactions on Plasma Science*, 36, 1168-1169, 10.1109/tps.2008.922424, 2008.
- Grimmich, N., Plaschke, F., Grison, B., Prencipe, F., Escoubet, C. P., Archer, M. O., ... Maggiolo, R: Cluster Magnetopause Crossings between 2001 and 2020 [dataset], <https://doi.org/10.17605/OSF.IO/PXCTG>, 2024.
- Gu, Y. X., Wang, Y., Wei, F. S., Feng, X. S., Song, X. J., Wang, B. Y., Zuo, P. B., Jiang, C. W., Xu, X. J., and Zhou, Z. L.: Quasi-elastodynamic Processes Involved in the Interaction between Solar Wind and Magnetosphere, *The Astrophysical Journal*, 946, 102, 10.3847/1538-4357/acbe9b, 2023.
- Haerendel, G.: Field-Aligned Currents in the Earth's Magnetosphere, in: *Physics of Magnetic Flux Ropes*, *Geophysical Monograph Series*, 539-553, <https://doi.org/10.1029/GM058p0539>, 1990.
- Harterting, M. D., Turner, D. L., Plaschke, F., Angelopoulos, V., and Singer, H.: The role of transient ion foreshock phenomena in driving Pc5 ULF wave activity, *Journal of Geophysical Research: Space Physics*, 118, 299-312, <https://doi.org/10.1029/2012JA018349>, 2013.

- Hu, Y.-Q., Guo, X.-C., Li, G.-Q., Wang, C., and Huang, Z.-H.: Oscillation of Quasi-Steady Earth's Magnetosphere, 22, 2723, 10.1088/0256-307x/22/10/073, 2005.
- Kepko, L. and Spence, H. E.: Observations of discrete, global magnetospheric oscillations directly driven by solar wind density variations, *Journal of Geophysical Research-Space Physics*, 108, 10.1029/2002ja009676, 2003.
- 560 Kivelson, M. G., Etcheto, J., and Trotignon, J. G.: Global compressional oscillations of the terrestrial magnetosphere: The evidence and a model, 89, 9851-9856, <https://doi.org/10.1029/JA089iA11p09851>, 1984.
- Kruskal, M. and Schwarzschild, M.: SOME INSTABILITIES OF A COMPLETELY IONIZED PLASMA, *Proceedings of the Royal Society of London Series a-Mathematical and Physical Sciences*, 223, 348-360, 10.1098/rspa.1954.0120, 1954.
- Lepping, R. P., Acuña, M. H., Burlaga, L. F., Farrell, W. M., Slavin, J. A., Schatten, K. H., Mariani, F., Ness, N. F., Neubauer, F. M., Whang, Y. C., Byrnes, J. B., Kennon, R. S., Panetta, P. V., Scheifele, J., and Worley, E. M.: The WIND magnetic field investigation, *Space Science Reviews*, 71, 207-229, 10.1007/BF00751330, 1995.
- 565 Lin, R., Anderson, K., Ashford, S., Carlson, C., Curtis, D., Ergun, R., Larson, D., McFadden, J., McCarthy, M., and Parks, G. J. S. S. R.: A three-dimensional plasma and energetic particle investigation for the Wind spacecraft, 71, 125-153, 1995.
- Lin, R. L., Zhang, X. X., Liu, S. Q., Wang, Y. L., and Gong, J. C.: A three-dimensional asymmetric magnetopause model, 115, 570 <https://doi.org/10.1029/2009JA014235>, 2010.
- Lyon, J. G., Fedder, J. A., and Mobarry, C. M.: The Lyon-Fedder-Mobarry (LFM) global MHD magnetospheric simulation code, *Journal of Atmospheric and Solar-Terrestrial Physics*, 66, 1333-1350, 10.1016/j.jastp.2004.03.020, 2004.
- Mann, I. R., Murphy, K. R., Ozeke, L. G., Rae, I. J., Milling, D. K., Kale, A. A., and Honary, F. F.: The Role of Ultralow Frequency Waves in Radiation Belt Dynamics, in: *Dynamics of the Earth's Radiation Belts and Inner Magnetosphere*, 69-92, 575 <https://doi.org/10.1029/2012GM001349>, 2012.
- Matsuoka, H., Takahashi, K., and Yumoto, K.: Observation and modeling of compressional Pi 3 magnetic pulsations, 100, 10.1029/94JA03368, 1995.
- McFadden, J., Carlson, C., Larson, D., Ludlam, M., Abiad, R., Elliott, B., Turin, P., Marckwordt, M., and Angelopoulos, V.: The THEMIS ESA plasma instrument and in-flight calibration, *Space Science Reviews*, 141, 277-302, 10.1007/s11214-008-580 9440-2, 2008.
- Mead, G. D. and Beard, D. B.: Shape of the geomagnetic field solar wind boundary, *Journal of Geophysical Research*, 69, 1169-1179, 10.1029/jz069i007p01169, 1964.
- Merkin, V. G. and Lyon, J. G.: Effects of the low-latitude ionospheric boundary condition on the global magnetosphere, *Journal of Geophysical Research: Space Physics*, 115, <https://doi.org/10.1029/2010JA015461>, 2010.
- 585 Moritaka, T., Kajimura, Y., Usui, H., Matsumoto, M., Matsui, T., and Shinohara, I.: Momentum transfer of solar wind plasma in a kinetic scale magnetosphere, *Physics of Plasmas*, 19, 10.1063/1.3683560, 2012.
- Mottez, F.: Relationship between Alfvén Wave and Quasi-Static Acceleration in Earth's Auroral Zone, in: *Low-Frequency Waves in Space Plasmas*, 121-138, <https://doi.org/10.1002/9781119055006.ch8>, 2016.
- Olson, W. P.: The shape of the tilted magnetopause, 74, 5642-5651, <https://doi.org/10.1029/JA074i024p05642>, 1969.

- 590 Omelchenko, Y. A., Roytershteyn, V., Chen, L. J., Ng, J., and Hietala, H.: HYPERS simulations of solar wind interactions with the Earth's magnetosphere and the Moon, *Journal of Atmospheric and Solar-Terrestrial Physics*, 215, 10.1016/j.jastp.2021.105581, 2021.
- P. Song, B. U. d. S., and M. F. Thomsen, Eds. : *Physics of the Magnetopause*, 5260, 364-364 pp., doi:10.1126/science.272.5260.364.a, 1996.
- 595 Petrinec, S. M.: Nowcasting and Forecasting the Magnetopause and Bow Shock Locations Based on Empirical Models and Real-Time Solar Wind Data, in: *Space Weather*, 257-263, <https://doi.org/10.1029/GM125p0257>, 2001.
- Petrinec, S. M. and Russell, C. T.: Near-Earth magnetotail shape and size as determined from the magnetopause flaring angle, 101, 137-152, <https://doi.org/10.1029/95JA02834>, 1996.
- Plaschke, F.: ULF Waves at the Magnetopause, in: *Low - Frequency Waves in Space Plasmas*, 193-212, 600 <https://doi.org/10.1002/9781119055006.ch12>, 2016.
- Plaschke, F., Glassmeier, K. H., Sibeck, D. G., Auster, H. U., Constantinescu, O. D., Angelopoulos, V., and Magnes, W.: Magnetopause surface oscillation frequencies at different solar wind conditions, *Annales Geophysicae*, 27, 4521-4532, 10.5194/angeo-27-4521-2009, 2009a.
- Plaschke, F., Glassmeier, K.-H., Auster, H. U., Constantinescu, O. D., Magnes, W., Angelopoulos, V., Sibeck, D. G., and 605 McFadden, J. P.: Standing Alfvén waves at the magnetopause, 36, <https://doi.org/10.1029/2008GL036411>, 2009b.
- Powell, K. G., Roe, P. L., Linde, T. J., Gombosi, T. I., and De Zeeuw, D. L.: A solution-adaptive upwind scheme for ideal magnetohydrodynamics, *Journal of Computational Physics*, 154, 284-309, 10.1006/jcph.1999.6299, 1999.
- Raeder, J., McPherron, R. L., Frank, L. A., Kokubun, S., Lu, G., Mukai, T., Paterson, W. R., Sigwarth, J. B., Singer, H. J., and Slavin, J. A.: Global simulation of the Geospace Environment Modeling substorm challenge event, *Journal of Geophysical* 610 *Research: Space Physics*, 106, 381-395, <https://doi.org/10.1029/2000JA000605>, 2001.
- RÈMe, H., Bosqued, J. M., Sauvaud, J. A., Cros, A., Dandouras, J., Aoustin, C., Bouyssou, J., Camus, T., Cuvilo, J., Martz, C., MÉDale, J. L., Perrier, H., Romefort, D., Rouzaud, J., D'Uston, C., MöBius, E., Crocker, K., Granoff, M., Kistler, L. M., Popecki, M., Hovestadt, D., Klecker, B., Paschmann, G., Scholer, M., Carlson, C. W., Curtis, D. W., Lin, R. P., McFadden, J. P., Formisano, V., Amata, E., Bavassano-Cattaneo, M. B., Baldetti, P., Belluci, G., Bruno, R., Chionchio, G., Di Lellis, A., 615 Shelley, E. G., Ghielmetti, A. G., Lennartsson, W., Korth, A., Rosenbauer, H., Lundin, R., Olsen, S., Parks, G. K., McCarthy, M., and Balsiger, H.: THE CLUSTER ION SPECTROMETRY (CIS) EXPERIMENT, *Space Science Reviews*, 79, 303-350, 10.1023/A:1004929816409, 1997.
- Russell, C. T.: The structure of the magnetopause, *Planetary and Space Science*, 51, 731-744, 10.1016/s0032-0633(03)00110-7, 2003.
- 620 Samson, J. C., Harrold, B. G., Ruohoniemi, J. M., Greenwald, R. A., and Walker, A. D. M.: FIELD LINE RESONANCES ASSOCIATED WITH MHD WAVE-GUIDES IN THE MAGNETOSPHERE, *Geophysical Research Letters*, 19, 441-444, 10.1029/92gl00116, 1992.

- Samsonov, A. A., Bogdanova, Y. V., Branduardi-Raymont, G., Sibeck, D. G., and Toth, G.: Is the Relation Between the Solar Wind Dynamic Pressure and the Magnetopause Standoff Distance so Straightforward?, *Geophysical Research Letters*, 47, e2019GL086474, <https://doi.org/10.1029/2019GL086474>, 2020.
- Samsonov, A. A., Gordeev, E., Tsyganenko, N. A., Šafránková, J., Němeček, Z., Šimůnek, J., Sibeck, D. G., Tóth, G., Merkin, V. G., and Raeder, J.: Do we know the actual magnetopause position for typical solar wind conditions?, *Journal of Geophysical Research: Space Physics*, 121, 6493-6508, <https://doi.org/10.1002/2016JA022471>, 2016.
- Sato, H., Pécseli, H., Trulsén, J., Sandholt, P. E., and Farrugia, C.: Impulse-driven oscillations of the near-Earth's magnetosphere, *Ann. Geophys.*, 40, 641-663, 10.5194/angeo-40-641-2022, 2022.
- Schild, M. A.: Pressure balance between solar wind and magnetosphere, 74, 1275-1286, <https://doi.org/10.1029/JA074i005p01275>, 1969.
- Shue, J.-H., Song, P., Russell, C. T., Steinberg, J. T., Chao, J. K., Zastenker, G., Vaisberg, O. L., Kokubun, S., Singer, H. J., Detman, T. R., and Kawano, H.: Magnetopause location under extreme solar wind conditions, 103, 17691-17700, <https://doi.org/10.1029/98JA01103>, 1998.
- Shue, J. H., Chao, J. K., Fu, H. C., Russell, C. T., Song, P., Khurana, K. K., and Singer, H. J.: A New Functional form to Study the Solar Wind Control of the Magnetopause Size and Shape, *Journal of Geophysical Research*, 102, 9497, 10.1029/97ja00196, 1997.
- Shue, J. H., Chen, Y. S., Hsieh, W. C., Nowada, M., Lee, B. S., Song, P., Russell, C. T., Angelopoulos, V., Glassmeier, K. H., McFadden, J. P., and Larson, D.: Uneven compression levels of Earth's magnetic fields by shocked solar wind, *Journal of Geophysical Research: Space Physics*, 116, n/a-n/a, 10.1029/2010ja016149, 2011.
- Sibeck, D. G.: The Magnetospheric and Ionospheric Response to Solar Wind Dynamic Pressure Variations, in: *Modeling Magnetospheric Plasma Processes*, 1-8, <https://doi.org/10.1029/GM062p0001>, 1991.
- Sibeck, D. G., Silveira, M. V. D., and Collier, M. R.: Tracking the Subsolar Bow Shock and Magnetopause, 127, e2022JA030704, <https://doi.org/10.1029/2022JA030704>, 2022.
- Sibeck, D. G., Baumjohann, W., Elphic, R. C., Fairfield, D. H., Fennell, J. F., Gail, W. B., Lanzerotti, L. J., Lopez, R. E., Luehr, H., Lui, A. T. Y., MacLennan, C. G., McEntire, R. W., Potemra, T. A., Rosenberg, T. J., and Takahashi, K.: The Magnetospheric Response to 8-Minute Period Strong-Amplitude Upstream Pressure Variations, *Journal of Geophysical Research-Space Physics*, 94, 2505-2519, 10.1029/JA094iA03p02505, 1989.
- Silveira, M. V. D. and Sibeck, D. G.: A Linear Velocity Gradient in the Subsolar Magnetosheath, 128, e2023JA031362, <https://doi.org/10.1029/2023JA031362>, 2023.
- Silveira, M. V. D., Sibeck, D. G., Cardoso, F. R., and Gjerloev, J. W.: Tracking the Subsolar Bow Shock and Magnetopause: Applying the Magnetosheath Velocity Gradient Method, 129, e2023JA032166, <https://doi.org/10.1029/2023JA032166>, 2024.
- Smit, G. R.: Oscillatory motion of the nose region of the magnetopause, 73, 4990-4993, <https://doi.org/10.1029/JA073i015p04990>, 1968.

- Song, P., Elphic, R. C., and Russell, C. T.: ISEE-1 AND ISEE-2 OBSERVATIONS OF THE OSCILLATING MAGNETOPAUSE, *Geophysical Research Letters*, 15, 744-747, 10.1029/GL015i008p00744, 1988.
- Song, X., Zuo, P., and Zhou, Z.: Automatic Identification of Magnetopause Crossing Events, *Chinese Journal of Space Science*, 41, 375-383, 10.3724/SP.J.0254-6124.2021.0303, 2021.
- 660 Spreiter, J. R., Summers, A. L., and Alksne, A. Y.: Hydromagnetic flow around the magnetosphere, *Planetary and Space Science*, 14, 223-253, [https://doi.org/10.1016/0032-0633\(66\)90124-3](https://doi.org/10.1016/0032-0633(66)90124-3), 1966.
- Staples, F. A., Ashley, R. A., Forsyth, S. C., Jonathan, I., and Rae: THEMIS Magnetopause Crossing Database (1) [dataset], 10.5281/zenodo.3700504, 2020a.
- Staples, F. A., Rae, I. J., Forsyth, C., Smith, A. R. A., Murphy, K. R., Raymer, K. M., Plaschke, F., Case, N. A., Rodger, C. J.,
- 665 Wild, J. A., Milan, S. E., and Imber, S. M.: Do Statistical Models Capture the Dynamics of the Magnetopause During Sudden Magnetospheric Compressions?, *Journal of Geophysical Research: Space Physics*, 125, e2019JA027289, 10.1029/2019ja027289, 2020b.
- Tóth, G., Sokolov, I. V., Gombosi, T. I., Chesney, D. R., Clauer, C. R., De Zeeuw, D. L., Hansen, K. C., Kane, K. J., Manchester, W. B., Oehmke, R. C., Powell, K. G., Ridley, A. J., Roussev, I. I., Stout, Q. F., Volberg, O., Wolf, R. A., Sazykin,
- 670 S., Chan, A., Yu, B., and Kóta, J.: Space Weather Modeling Framework: A new tool for the space science community, *Journal of Geophysical Research: Space Physics*, 110, <https://doi.org/10.1029/2005JA011126>, 2005.
- Tsyganenko, N.: Effects of the Solar Wind Conditions on the Global Magnetospheric Configuration as Deduced From Data-Based Field Models, *European Space Agency, (Special Publication) ESA SP*, 389, 1996.
- Tsyganenko, N. A.: A magnetospheric magnetic field model with a warped tail current sheet, *Planetary and Space Science*, 37,
- 675 5-20, [https://doi.org/10.1016/0032-0633\(89\)90066-4](https://doi.org/10.1016/0032-0633(89)90066-4), 1989.
- Tsyganenko, N. A.: Empirical Magnetic Field Models for the Space Weather Program, in: *Space Weather*, 273-280, <https://doi.org/10.1029/GM125p0273>, 2001.
- Walker, R. J., Lapenta, G., Berchem, J., El-Alaoui, M., and Schriver, D.: Embedding particle-in-cell simulations in global magnetohydrodynamic simulations of the magnetosphere, *Journal of Plasma Physics*, 85, 10.1017/s0022377819000072, 2019.
- 680 Wang, Y. and Chen, C. X.: Numerical Simulation of Radial Plasma Transport in the Saturn's Magnetosphere, *Chinese Journal of Geophysics*, 51, 635-642, 10.1002/cjg2.1235, 2008.
- Willis, D. M.: Structure of the magnetopause, 9, 953-985, <https://doi.org/10.1029/RG009i004p00953>, 1971.
- Zong, Q., Escoubet, P., Sibeck, D., Le, G., and Zhang, H.: Dayside Magnetosphere Interactions, in: *Dayside Magnetosphere Interactions*, 303-306, <https://doi.org/10.1002/9781119509592.ch17>, 2020.

685